Machine learning-based non-invasive prediction of atrial fibrillation driver location and ablation outcome using the 12-lead ECG

-

Supplementary Material

Giorgio Luongo (MSc)[1], Luca Azzolin (MSc)[1], Steffen Schuler (MSc)[1], Massimo W Rivolta (PhD)[2], Tiago P Almeida (PhD)[3], Juan P Martínez (PhD)[4], Diogo C Soriano (PhD)[5], Armin Luik (MD)[6], Amir Jadidi (MD)[7], Olaf Dössel (PhD)[1], Roberto Sassi (PhD)[2], Pablo Laguna (PhD)[4], Axel Loewe (PhD)[1]

[1]*Institute of Biomedical Engineering, Karlsruhe Institute of Technology, Karlsruhe, Germany*
[2]*Dipartimento di Informatica, Università degli Studi di Milano, Milan, Italy*
[3]*Department of Cardiovascular Sciences, University of Leicester, Leicester, UK*
[4]*I3A, Universidad de Zaragoza, and CIBER-BNN, Zaragoza, Spain*
[5]*Engineering, Modelling and Applied Social Sciences Centre, ABC Federal University, São Bernardo do Campo, Brazil*
[6]*Medizinische Klinik IV, Städtisches Klinikum Karlsruhe, Karlsruhe, Germany*
[7]*Department of Electrophysiology, University-Heart-Center Freiburg-Bad Krozingen, Bad Krozingen Campus, Germany.*

Table 1: List of extracted features.

1. $\overline{\mathcal{H}_0}$	2. $\sigma^2_{\mathcal{H}_0}$	3. $\overline{\mathcal{H}_1}$	4. $\sigma^2_{\mathcal{H}_1}$	5. $\overline{\mathcal{H}_2}$	6. $\sigma^2_{\mathcal{H}_2}$	7. $\mathcal{D}_{VCG}$
8. $\mathcal{E}^{DL}_{VCG}$	9. $\mathcal{R}^{R}_{VCG}$	10. $\mathcal{L}_{VCG}$	11. $\mathcal{T}_{VCG}$	12. $\mathcal{E}^{VL}_{VCG}$	13-14. $\mathcal{D}_{srRQA_d}$	15-16. $\mathcal{E}^{DL}_{srRQA_d}$
17-18. $\mathcal{R}^{R}_{srRQA_d}$	19-20. $\mathcal{L}_{srRQA_d}$	21-22. $\mathcal{T}_{srRQA_d}$	23-24. $\mathcal{E}^{VL}_{srRQA_d}$	25-28. $\mathcal{R}^{R}_{idRQA_{PCi}}$	29-32. $\mathcal{D}_{idRQA_{PCi}}$	33-36. $\mathcal{L}_{idQA_{PCi}}$
37-40. $\mathcal{T}_{idRQA_{PCi}}$	41-44. $\mathcal{E}^{VL}_{idRQA_{PCi}}$	45-48. $\mathcal{E}^{DL}_{idRQA_{PCi}}$	49-60. $\overline{\lambda_i}$	61-72. σ_{λ_i}	73. $\overline{\lambda}_{PC}$	74. $\sigma_{\lambda_{PC}}$
75-86. $\overline{R}_i$	87-98. σ_{R_i}	99. $\overline{R}_{PC}$	100. $\sigma_{R_{PC}}$	101. $\overline{OI}$	102. σ_{OI}	103. $\overline{SE}$

1. Feature extraction methods

1.1. Hjort descriptors

The Hjort descriptors are closely related to the spectral moments. The first descriptor, $\mathcal{H}_0$, called activity, is defined by the total signal power. The second descriptor, $\mathcal{H}_1$, called mobility, reflects the dominant frequency of the signal under analysis. The third descriptor, $\mathcal{H}_2$, is used to define a measure related to half of the bandwidth of the signal and is termed complexity [1]. These descriptors were evaluated for each ECG lead. The mean values and the variances of these parameters over all 12 leads were calculated and used as features (feat. 1-6 in Table 1).

1.2. Recurrence quantification analysis on vectocardiogram

The vectocardiogram (VCG) was calculated from the 12-lead ECG using the Dower's inverse transformation, and the 3-D VCG vector loops were used as state space plots for a further recurrence quantification analysis (RQA) [2]. RQA allowed to analyse the topological structure of multidimensional dynamical systems, giving access to a signal's intermittency, regularity, and predictability [3]. A detailed explanation of the RQA and the respective extractable parameters can be found in the work of Marwan et al., [3]. The extracted parameters were: determinism ($\mathcal{D}_{VCG}$), entropy of the diagonal lines ($\mathcal{E}^{DL}_{VCG}$), recurrence rate ($\mathcal{R}^{R}_{VCG}$), laminarity ($\mathcal{L}_{VCG}$), trapping time ($\mathcal{T}_{VCG}$), and entropy of the vertical lines ($\mathcal{E}^{VL}_{VCG}$), (feat. 7-12 in Table 1).

1.3. spatial reduced RQA

From the 12-lead ECGs, the first four principal components (PCs) were extracted (representing more than 99% of the total variability). The first three PCs,

and the first four PCs, were used as dimensions (d) of a state space in which a spatial reduced RQA ($srRQA_3$ and $srRQA_4$) was applied, respectively [4]. The extracted parameters were: determinism ($\mathcal{D}_{srRQA_d}$), entropy of the diagonal lines ($\mathcal{E}^{DL}_{srRQA_d}$), recurrence rate ($\mathcal{R}^{R}_{srRQA_d}$), laminarity ($\mathcal{L}_{srRQA_d}$), trapping time ($\mathcal{T}_{srRQA_d}$), and entropy of the vertical lines ($\mathcal{E}^{VL}_{srRQA_d}$), (feat. 13-24 in Table 1).

1.4. individual component RQA

An individual component RQA (icRQA) was also applied on each of the first four PCs calculated from the 12-lead ECGs [4]. The extracted parameters were: determinism ($\mathcal{D}_{icRQA_{PCi}}$), entropy of the diagonal lines ($\mathcal{E}^{DL}_{icRQA_{PCi}}$), recurrence rate ($\mathcal{R}^{R}_{icRQA_{PCi}}$), laminarity ($\mathcal{L}_{icRQA_{PCi}}$), trapping time ($\mathcal{T}_{icRQA_{PCi}}$), and entropy of the vertical lines ($\mathcal{E}^{VL}_{icRQA_{PCi}}$), with i being the number of PC, (feat. 25-48 in Table 1).

1.5. Ratio PCA eigenvalues

The 12-lead ECGs were divided in 3 segments of the same length (i.e., 1 s considering the total length of each ECG of 3 s). For each segment j, the eigenvalues ($\lambda_{i,\,j}$) corresponding to the spatial principal component analysis (PCA) components over the 12 leads were extracted. From the $\lambda_{i,\,j}$, also the ratio was calculated:

$$R_{i,\,j} = \frac{\lambda_{i,\,j}}{\sum_{k \neq i} \lambda_{k,\,j}}, \tag{1}$$

with k being the number of PC.

The features extracted were: the mean λ values and the respective standard deviations for each PC over all segments ($\overline{\lambda_i}$ and σ_{λ_i}); from $\overline{\lambda_i}$, the mean over the 12 PCs and the respective standard deviation ($\overline{\lambda}_{PC}$ and $\sigma_{\lambda_{PC}}$); the mean R values and the respective standard deviations for each PC over all segments ($\overline{R}_i$ and σ_{R_i}); from $\overline{R}_i$, the mean over the 12 PCs and the respective standard deviation

($\overline{R}_{PC}$ and $\sigma_{R_{PC}}$), (feat. 49-100 in Table 1). The idea behind the $R_{i,j}$ parameter and the extracted features was to increase the differences between the eigenvalues to achieve a better discrimination due to the variability shown by the PCs over time and between them.

1.6. Organization index

The organization index (OI) was used as a measure of atrial fibrillation spatio-temporal organization, and it was computed as follows. The spectrum of each 12-lead ECGs was calculated. The areas under the five largest peaks of each spectrum were computed using a 1 Hz frequency interval centred on each peak. The OI was then defined as the ratio of the area under these five peaks to the total spectrum area [5] for each lead. The feature extracted were: the mean OI and the respective standard deviation over the leads ($\overline{OI}$ and σ_{OI}), (feat. 101-102 in Table 1).

1.7. Spectral entropy

The spectral entropy (SE) of a signal is a measure of its spectral power distribution. The concept is based on the Shannon entropy, or information entropy, in information theory. The SE treats the signal's normalized power distribution in the frequency domain as a probability distribution, and calculates the Shannon entropy of it. The Shannon entropy in this context is the spectral entropy of the signal [6]. The SE was calculated for each of the 12-leads with the MATLAB *pentropy* function and consecutively averaged along and between leads. The feature extracted was the mean SE over the leads ($\overline{SE}$), (feat. 103 in Table 1).

2. Clinical 12-lead ECG

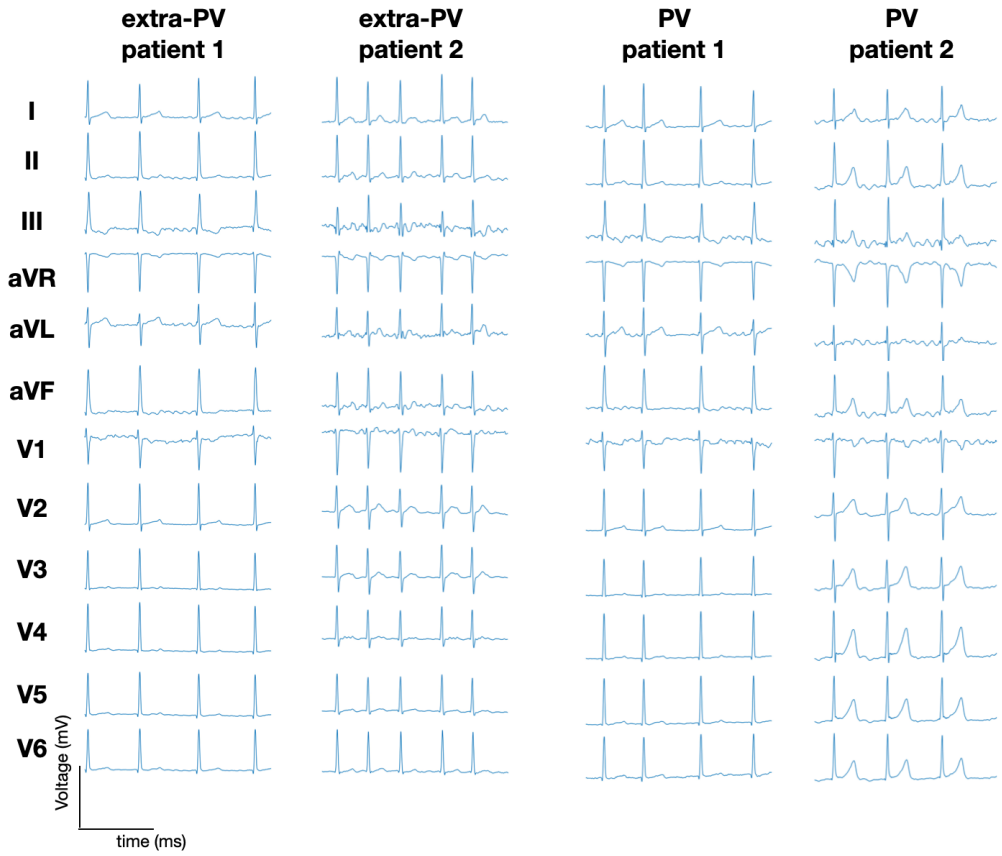

Figure 1: Examples of 12-lead ECGs from four representative clinical patients for the 2 classes (extra-PV class, left; PV class, right).

3. Alternative machine learning algorithm approaches

In this work, we focused on the implementation of a decision tree classifier for binary classification (AF drivers located at the PVs vs. extra-PV drivers) due to its simplicity and explainability. However, several machine learning approaches have been trained and tested (i.e., linear discriminant analysis - LDA, and radial

basis neural network - rbNN). The implementation and optimization of the classifiers followed the same procedure as described in the main text of this work for the decision tree (Section 2.5).

The binary LDA classifier achieved a G-Mean of 76.4±12.8% on the in silico test set with a sensitivity of 88.3±3.7%, a specificity of 66.1±17.1% on the simulated dataset (PV considered as the positive class). On the first unseen clinical dataset, the classifier achieved 71.7% G-Mean with a sensitivity of 69.6%, a specificity of 73.9%, and PPV of 72.7%. On the second clinical dataset the classifier achieved 68.4% G-Mean with a sensitivity of 69.6%, a specificity of 65.2%, and PPV of 66.6%.

The binary rbNN classifier achieved a G-Mean of 86.8±10.1% on the in silico test set with a sensitivity of 96.2±4.5%, a specificity of 78.4±16.3% on the simulated dataset (PV considered as the positive class). On the first unseen clinical dataset, the classifier achieved 78.1% G-Mean with a sensitivity of 69.6%, a specificity of 86.9%, and PPV of 84.2%. On the second clinical dataset the classifier achieved 69.6% G-Mean with a sensitivity of 69.6%, a specificity of 69.6%, and PPV of 69.6%.

4. Feature importance analysis

Shapley calculation was implemented to analyze a posteriori the importance of the 11 features selected for the binary PV vs. extra-PV classification once the model has been trained. In Fig. 2 we can see the Shapley values (the contribution that each feature gives to the classification). We can observe that the features gave all a positive contribution to the classification apart from two features that gave a slightly negative contribution (it was expected, being all good features). However,

the negative features have not been removed from the feature set since the removal of such features a posteriori could have brought to overfitting on the model.

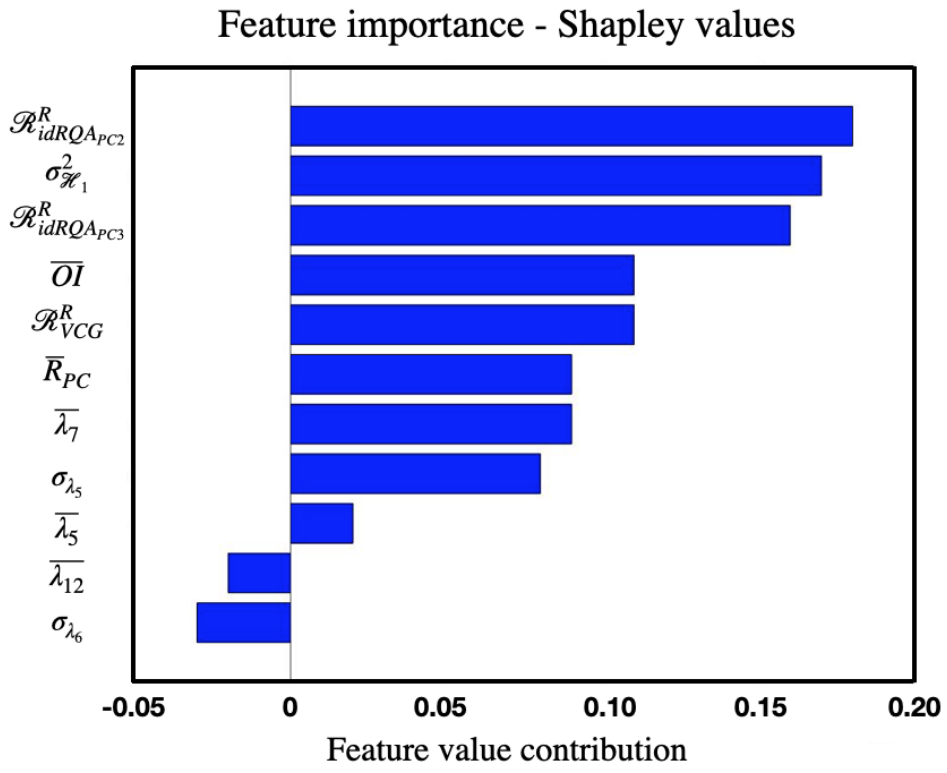

Figure 2: Shapley feature importance calculation on the 11 features selected for the binary classification PV vs. extra-PV AF drivers location.

5. Multivariate regression analysis

Multivariate regression analysis performed between the variables LVEF, LAD, renal dysfunction, sex, age, and our classifier (Table 2).

Table 2: Multivariate regression analysis.

	Regression coefficient B	Standard error	Wald	df	Significance	Hazard ratio
Age	-0.069	0.055	1.575	1	0.210	0.934
Sex	0.557	1.114	0.251	1	0.617	1.746
LAD	-0.090	0.106	0.720	1	0.396	0.914
LVEF	-3.104	7.444	0.174	1	0.677	0.045
Renal dysfunction	1.982	1.216	2.655	1	0.103	7.256
Classifier	2.468	1.252	3.887	1	0.049	11.795
Constant	7.929	8.415	0.888	1	0.346	2777.043

6. Consistency analysis

A consistency analysis was implemented by running the classifier on a new ECG set composed of the same 46 patients but different ECG segments than those used in the clinical dataset showed in the main manuscript. In Table 3, the confusion matrix obtained on the "consistency" ECG set.

Table 3: Confusion matrix of the clinical set of different ECG segments extracted from the same 46 patients for a consistency analysis for PV vs. extra-PV AF driver location classification.

		True class	
		PV	extra-PV
Predicted class	PV	16	6
	extra-PV	7	17

References

[1] L. Sörnmo, P. Laguna, Chapter 3 - eeg signal processing, in: L. Sörnmo, P. Laguna (Eds.), Bioelectrical Signal Processing in Cardiac and Neurological Applications, Biomedical Engineering, Academic Press, Burlington, 2005, pp. 55 – 179. doi:10.1016/B978-012437552-9/50003-9.

[2] H. Yang, Multiscale recurrence quantification analysis of spatial cardiac vectocardiogram signals, IEEE Trans. Biomed. Eng. 58 (2) (2011) 339–347. doi:10.1109/TBME.2010.2063704.

[3] N. Marwan, M. Carmen Romano, M. Thiel, J. Kurths, Recurrence plots for the analysis of complex systems, Physics Reports 438 (5) (2007) 237 – 329. doi:10.1016/j.physrep.2006.11.001.

[4] G. Luongo, S. Schuler, A. Luik, et al., Non-invasive characterization of atrial flutter mechanisms using recurrence quantification analysis on the ECG: a computational study, IEEE Trans. Biomed. Eng.doi:10.1109/TBME.2020.2990655.

[5] L. Uldry, J. Van Zaen, Y. Prudat, L. Kappenberger, J.-M. Vesin, Measures of spatiotemporal organization differentiate persistent from long-standing atrial fibrillation, EP Europace 14 (8) (2012) 1125–1131. doi:10.1093/europace/eur436.

[6] A. Vakkuri, A. Yli-Hankala, P. Talja, et al., Time-frequency balanced spectral entropy as a measure of anesthetic drug effect in central nervous system during sevoflurane, propofol, and thiopental anesthesia, Acta Anaesthesiologica

Scandinavica 48 (2) (2004) 145–153. doi:10.1111/j.0001-5172.2004.00323.x.